JVI Journals.ASM.org

Severe Acute Respiratory Syndrome Coronavirus Protein nsp1 Is a Novel Eukaryotic Translation Inhibitor That Represses Multiple Steps of Translation Initiation

Kumari G. Lokugamage,[a] Krishna Narayanan,[a] Cheng Huang,[a] and Shinji Makino[a,b,c,d]

Department of Microbiology and Immunology,[a] Center for Biodefense and Emerging Infectious Diseases,[b] UTMB Center for Tropical Diseases,[c] and Sealy Center for Vaccine Development,[d] The University of Texas Medical Branch, Galveston, Texas, USA

Severe acute respiratory syndrome (SARS) coronavirus nonstructural protein 1 (nsp1) binds to the 40S ribosomal subunit and inhibits translation, and it also induces a template-dependent endonucleolytic cleavage of host mRNAs. nsp1 inhibits the translation of cap-dependent and internal ribosome entry site (IRES)-driven mRNAs, including SARS coronavirus mRNAs, hepatitis C virus (HCV), and cricket paralysis virus (CrPV) IRES-driven mRNAs that are resistant to nsp1-induced RNA cleavage. We used an nsp1 mutant, nsp1-CD, lacking the RNA cleavage function, to delineate the mechanism of nsp1-mediated translation inhibition and identify the translation step(s) targeted by nsp1. nsp1 and nsp1-CD had identical inhibitory effects on mRNA templates that are resistant to nsp1-induced RNA cleavage, implying the validity of using nsp1-CD to dissect the translation inhibition function of nsp1. We provide evidence for a novel mode of action of nsp1. nsp1 inhibited the translation initiation step by targeting at least two separate stages: 48S initiation complex formation and the steps involved in the formation of the 80S initiation complex from the 48S complex. nsp1 had a differential, mRNA template-dependent, inhibitory effect on 48S and 80S initiation complex formation. nsp1 inhibited different steps of translation initiation on CrPV and HCV IRES, both of which initiate translation via an IRES-40S binary complex intermediate; nsp1 inhibited binary complex formation on CrPV IRES and 48S complex formation on HCV IRES. Collectively, the data revealed that nsp1 inhibited translation by exerting its effect on multiple stages of translation initiation, depending on the mechanism of initiation operating on the mRNA template.

Severe acute respiratory syndrome (SARS) coronavirus (SCoV) is the causative agent of the respiratory disease SARS, which emerged in southern China in 2002 and spread to different countries of the world during a 2002–2003 epidemic (6, 18–20, 26, 30). SCoV carries a large, single-stranded, positive-sense RNA genome. The 5′-most two-thirds of the genome contains two large overlapping open reading frames that encode two polyproteins, which are cleaved by virus-encoded proteinases into 16 nonstructural proteins (nsp1 to nsp16), most of which are involved in viral RNA synthesis.

Coronavirus (CoV) nsp1 proteins share a biological function to inhibit host gene expression; nsp1 of different CoVs employ different strategies to inhibit host gene expression (11, 15, 16, 36). Several lines of evidence indicate a strong possibility that CoV nsp1 is a major CoV virulence factor (22, 36, 37, 39). SCoV nsp1 suppresses the host innate immune functions by inhibiting type I interferon expression (22) and host antiviral signaling pathways (37) in infected cells. Mouse hepatitis virus nsp1 inhibits the type I interferon system, and a mutant virus lacking the nsp1 gene is severely attenuated in infected mice (39). Hence, studies using CoV nsp1 proteins have begun to tease out the common as well as the divergent mechanisms involved in the CoV-induced inhibition of host gene expression and expanded our understanding of CoV virulence and pathogenesis.

SCoV nsp1 inhibits host protein synthesis and promotes the degradation of host mRNAs (16, 22) using a two-pronged strategy (15); by binding to the 40S ribosomal subunit, nsp1 suppresses translation and induces template-dependent endonucleolytic RNA cleavage of mRNA templates. nsp1 induces RNA cleavage in nonviral capped mRNAs and mRNAs carrying picornavirus type I and type II internal ribosome entry sites (IRESes), whereas it does not induce the RNA cleavage in SCoV mRNAs and RNA transcripts carrying IRES of cricket paralysis virus (CrPV), hepatitis C virus (HCV), or classical swine fever virus (12, 15). However, nsp1 is able to suppress the translation of all of the above mRNAs, suggesting that the translation inhibition activity of nsp1 is not dependent on its ability to induce RNA cleavage and inactivate the translational competence of the mRNA template.

To dissect the translation inhibition function of nsp1 and identify the step(s) in translation inhibited by nsp1, we isolated and characterized an nsp1 mutant lacking the RNA cleavage function that allowed us to delineate the mechanism of nsp1-mediated translation inhibition in the absence of nsp1-induced template mRNA cleavage. Our data revealed that nsp1, through its association with the 40S ribosomal subunit, inhibited the translation of both cap-dependent and IRES-driven template mRNAs at the translation initiation step. Interestingly, nsp1 exhibited a novel mode of action, wherein it inhibited multiple steps of translation initiation and the initiation step targeted by nsp1 was template mRNA dependent. Furthermore, our study suggested the presence of multiple mechanisms by which mRNA templates are resistant to nsp1-induced RNA cleavage.

Received 27 July 2012 **Accepted** 27 September 2012
Published ahead of print 3 October 2012
Address correspondence to Shinji Makino, shmakino@utmb.edu.

doi:10.1128/JVI.01958-12

MATERIALS AND METHODS

Plasmid construction. For expression of a mutant nsp1, nsp1-CD (the acronym CD stands for cleavage defective), in cultured cells, pCAGGS-nsp1-CD, carrying R124A and K125A mutations and a C-terminal myc tag, was constructed from the pCAGGS plasmid that encodes nsp1 (16) by using a recombinant PCR-based method. Insertion of the nsp1-CD gene into pcDNA 3.1 HisA myc and pGEX vector (GE Health care) resulted in generation of pcDNA-nsp1-CD, which was used for the *in vitro* synthesis of RNA transcripts encoding nsp1-CD, and pGEX-nsp1-CD, which was used for the expression of nsp1 in *Escherichia coli*, respectively. Plasmid pRL-leaderless-rluc was generated by inserting the T7 promoter and rLuc gene into pRL-SV40 (Promega). Sequence analyses of the plasmids confirmed the presence of the expected sequence.

Expression and purification of recombinant proteins. Glutathione *S*-transferase (GST)-fused proteins were expressed in BL21-CodonPlus DE3 *E. coli* cells (Stratagene) and purified by affinity purification using glutathione Sepharose 4B (GE Healthcare). GST tag was removed from the GST-fused proteins using PreScission protease (GE Healthcare).

***In vitro* transcription and RNA transfection.** Capped and polyadenylated RNA transcripts encoding chloramphenicol acetyltransferase (CAT), nsp1, nsp1-CD, or nsp1-mt were synthesized from linearized plasmids using the mMESSAGE mMACHINE T7 Ultra kit (Ambion). Synthesis of SCoV mRNA 9 was performed as described previously (12). HCV-rLuc RNA was synthesized from the PCR products obtained from HCV16Luc plasmid, while other IRES-containing RNAs were synthesized from the plasmids using the MEGAscript T7 kit (Applied Biosystems). Subconfluent 293 cells in 6-well plates were transfected with the transcripts using TransIT mRNA (Mirus).

Radiolabeling of intracellular proteins. Subconfluent 293 cells were transfected with *in vitro*-synthesized RNA transcripts. The cells were incubated with medium containing 4 μg/ml actinomycin D from 1 to 8 h posttransfection. Subsequently, the cells were incubated with methionine-free medium for 30 min and then metabolically labeled with 20 μCi/ml of Tran^{35}S-label (1,000 Ci/mmol; MP Biomedicals) for 1 h. The cell extracts were prepared by lysing the cells in sodium dodecyl sulfate-polyacrylamide gel electrophoresis (SDS-PAGE) sample buffer, and equivalent amounts of the extracts were analyzed on 12% SDS-PAGE gels.

Western blot analysis. Western blot analysis was performed as described previously (15). Anti-myc (Millipore), anti-S6 (Cell Signaling Technology), and anti-actin (Sigma) were used as primary antibodies. Goat anti-mouse IgG-horseradish peroxidase (HRP), goat anti-rabbit IgG-HRP, and donkey anti-goat IgG-HRP (Santa Cruz Biotech) were used as secondary antibodies.

Reporter gene assay. Subconfluent 293 cells grown in 24-well plates were cotransfected, in triplicate, with pRL-SV40 reporter plasmid (0.1 μg/well) and pCAGGS-based plasmid expressing CAT, nsp1-wt, a biologically inactive nsp1 mutant, nsp1-mt, or nsp1-CD (0.4 μg/well) using TransIT-293 reagent (Mirus). At 30 h posttransfection, cells were lysed and rLuc activities were measured.

Coimmunoprecipitation analysis. At 8 h after RNA transfection, cell lysates were prepared by using a buffer containing 50 mM Tris-HCl (pH 7.5), 5 mM $MgCl_2$, 100 mM KCl, and 1% Triton-X, incubated with anti-myc antibody (Millipore) at 4°C for 1 h, followed by incubation with Protein G Plus-Agarose (Santa Cruz Biotech) overnight at 4°C. After washing the samples four times with a buffer containing 10 mM HEPES (pH 7.4), 500 mM KCl, 2.5 mM $MgCl_2$, and 1 mM dithiothreitol, the pellets were subjected to Western blot analysis using anti-His (Santa Cruz) or anti-S6 (Cell Signaling) primary antibody.

***In vitro* translation and luciferase assay.** Rabbit reticulocyte lysate (RRL) (Retic Lysate IVT kit [Ambion]) were preincubated with GST, nsp1, nsp1-mt, or nsp1-CD proteins for 10 min at 30°C. Subsequently, *in vitro*-synthesized RNA transcripts were added to the RRL, and the samples were incubated for 10 min at 30°C. Aliquots of the translation reactions were diluted in *Renilla* luciferase assay lysis buffer (Promega), mixed with the *Renilla* luciferase assay reagent, and subjected to measurement of the luminescence.

Northern blot analysis. Northern blot analysis was performed using digoxigenin-labeled probes as described previously (16).

SGC analyses. The sucrose gradient centrifugation (SGC) analysis of 48S and 80S complexes in RRL was performed as described previously (3). The radioactivity in each fraction was measured and expressed as a percentage of the total radioactivity in the gradient. The percentage reduction in the ribosomal peaks, corresponding to the binary, 48S, and 80S complexes, in the presence of nsp1 and nsp1-CD was calculated relative to the control GST sample. The average inhibitory percentages shown in the text were calculated from three independent experiments. The values are represented as averages ± standard deviations. Binary IRES-40S subunit complexes were assembled by incubating [α-^{32}P]UTP-labeled HCV-rLuc RNA or [α-^{32}P]CTP-labeled CrPV-fLuc RNA with purified 40S subunits, which had been preincubated with GST, nsp1, or nsp1-CD, for 20 min at 30°C. 80S complexes were assembled by incubating purified 60S subunits and radiolabeled CrPV-fLuc RNA with 40S ribosomal subunits, which had been preincubated with GST, nsp1, or nsp1-CD, for 20 min at 30°C.

Toeprinting assays. Toeprinting assays were performed as described previously (15, 17, 24), with minor modifications. The sequence of 5′ ^{32}P-labeled primers and RNAs used with the primer are the following: 5′-TTT TTC TGA ATC ATA ATA ATT AA-3′ for leaderless rLuc RNA, GLA RNA (12), and HCV-rLuc RNA; 5′-AGC AAT TGT TCC AGG AAC CAG GG-3′ for EMCV-fLuc RNA and CrPV-fLuc RNA; and 5′-GTC CTC CAT TCT GGT TAT TGT C −3′ for SCoV mRNA9. The RRL were preincubated with GST, nsp1, nsp1-mt, or nsp1-CD for 10 min at 30°C. The samples were then incubated with either 1 mM GMP-PNP, a nonhydrolyzable GTP analog, or 0.6 mM cycloheximide (CHX) for 5 min at 30°C. The 5′-labeled primer was incubated with *in vitro*-synthesized RNA transcripts for 1 min at 65°C and then at 37°C for 8 min to generate primer-RNA complexes. The primer-RNA complexes were then added to the samples and capped, and EMCV-fLuc RNA-containing samples were incubated for 10 min at 30°C while the samples with HCV-rLuc RNA were incubated for 20 min at 30°C. The reactions were diluted 20-fold with a buffer containing 0.5 mM CHX, 7 mM magnesium acetate, 100 mM KCl, 0.5 mM dATP, dCTP, dGTP, and dTTP, 20 mM Tri-HCl (pH 7.4), 2 mM dithiothreitol, and 2 U/μl SuperScript III (Invitrogen) and incubated for 10 min at 30°C. We resolved the extracted primer extension products on an 8% sequencing gel. For toeprint analysis of binary complexes, purified 40S subunits were used in place of RRL and GMP-PNP or CHX was not added to the samples. After adding the primer-RNA complexes, the samples were incubated for 20 min at 30°C. For toeprint analysis of 80S complex formation on CrPV-fLuc RNA, the purified 40S subunits were preincubated with GST, nsp1, nsp1-mt, or nsp1-CD in the absence of GMP-PNP or CHX. The primer-RNA complex and purified 60S subunits were added to the sample and incubated for 20 min at 30°C. Band intensities of the binary complex and 48S- and 80S-specific toeprint signals were measured by densitometric scanning of the autoradiographs. The percent reduction in the toeprint signals in the presence of nsp1 and nsp1-CD was calculated relative to the control GST sample. We used three independent experimental measurements to calculate the average inhibitory percentages shown in the text. The values are represented as averages ± standard deviations.

Purification of ribosomal subunits. Ribosomal subunits were purified from RRL (Green Hectares, Oregon, WI) using a procedure previously described (29). Western blot analysis verified the absence of eIF2α, eIF3α, and eIF3β from the purified 40S subunit preparation (data not shown). The purity of the ribosomal subunits was also confirmed by the absence of 28S and 18S rRNA in the purified 40S and 60S subunit preparations, respectively.

Cosedimentation of nsp1-40S complex. Purified 40S subunits were incubated with nsp1 or nsp1-mt for 20 min at 30°C in a buffer containing 20 mM Tris-HCl, pH 7.5, 2 mM dithiothreitol, 2 mM $MgCl_2$, and 100 mM KCl and sedimented through 10 to 40% sucrose gradients in the same

buffer at 38,000 rpm for 3.5 h in a Beckman SW41 rotor. Fractions were collected, one-fourth of each fraction was precipitated with trichloroacetic acid, and proteins were visualized by Western blot analysis, while the rest was used to extract RNA and was subjected to Northern blot analysis using digoxigenin-labeled oligonucleotide probes to detect 18S rRNA.

RESULTS

Identification of an nsp1 mutant that inhibits translation but lacks the mRNA cleavage function. To gain insight into the mechanism of SCoV nsp1-mediated translation inhibition, we aimed to isolate an nsp1 mutant(s) that exhibits the translation inhibition activity but lacks the mRNA cleavage function of nsp1. We tested a series of nsp1 mutants, each carrying alanine substitution(s) of the charged amino acid residue(s) exposed on the surface of nsp1 (1), for their ability to inhibit host translation and induce an endonucleolytic cleavage in Ren-EMCV-FF RNA, a bicistronic reporter mRNA carrying the encephalomyocarditis virus (EMCV) IRES between the upstream Renilla luciferase (rLuc) gene and the downstream Firefly luciferase (fLuc) gene (11, 15). Using this method, we identified an nsp1 mutant, nsp1-CD, carrying R124A and K125A mutations, with the desired properties. In cells cotransfected with nsp1 expression plasmid and the reporter plasmid carrying the simian virus 40 promoter-driven rLuc gene (16), nsp1-CD inhibited rLuc reporter gene expression as efficiently as nsp1, whereas a biologically inactive nsp1 mutant, nsp1-mt, which does not bind to the 40S ribosomal subunit (22), did not suppress the reporter gene expression (Fig. 1A). nsp1-CD accumulated to a slightly higher level than nsp1, but its levels were lower than those of nsp1-mt (Fig. 1A), suggesting that, like nsp1 (22), nsp1-CD inhibited its own expression. nsp1 promotes host mRNA degradation (16); mRNAs that undergo nsp1-induced endonucleolytic RNA cleavage are subsequently degraded by the cellular exonuclease Xrn1 (9). nsp1 expression resulted in a marked reduction in the abundance of expressed reporter rLuc RNA and endogenous glyceraldehyde 3-phosphate dehydrogenase (GAPDH) mRNA, whereas nsp1-CD expression resulted in only a moderate reduction in rLuc RNA levels and had little effect on GAPDH mRNA abundance (Fig. 1B). Metabolic radiolabeling experiments with [^{35}S]methionine/cysteine showed that both nsp1 and nsp1-CD, but not nsp1-mt, inhibited host protein synthesis, with nsp1 displaying a stronger inhibitory effect than nsp1-CD (Fig. 2). Importantly, nsp1, but not nsp1-CD, induced an endonucleolytic RNA cleavage in REN-EMCV-FF in cultured cells (Fig. 3) (11), demonstrating that nsp1-CD lacked the endonucleolytic RNA cleavage function. Coimmunoprecipitation analysis of extracts, from cells expressing a C-terminal myc-His epitope-tagged nsp1, nsp1-mt, nsp1-CD, or CAT, with anti-myc antibody under stringent washing conditions showed the coimmunoprecipitation of the 40S ribosomal subunit with nsp1 and nsp1-CD but not nsp1-mt or CAT (Fig. 4). These data demonstrated that both nsp1 (15) and nsp1-CD, but not nsp1-mt or CAT, were tightly associated with the 40S ribosomal subunit.

We next tested the biological activity of purified nsp1-CD in the RRL *in vitro* translation system; purified nsp1, nsp1-mt, and GST served as controls, and purified nsp1 and its mutants carried a C-terminal myc-His tag (15). GLA RNA transcripts (12), encoding the rLuc gene carrying the 53-nucleotide (nt)-long 5′ untranslated region (UTR) of rabbit β-globin mRNA, were incubated in RRL in the presence of nsp1, nsp1-CD, nsp1-mt, or GST. A portion of the sample was used for the reporter assay, which showed

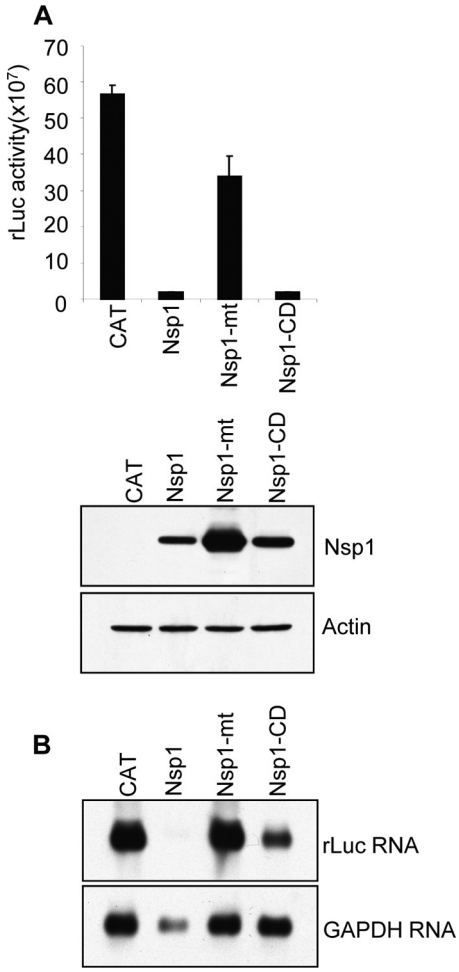

FIG 1 nsp1-CD inhibits reporter gene expression. 293 cells were cotransfected with pCAGGS-nsp1-CD (encoding nsp1-CD) and pRL-SV40 (encoding the rLuc gene). As a control, pCAGGS-CAT (encoding the CAT gene), pCAGGS-nsp1 (encoding nsp1), or pCAGGS-nsp1-mt (encoding biologically inactive nsp1-mt) was used in place of pCAGGS-nsp1-CD. Expressed nsp1, nsp1-mt, and nsp1-CD, but not CAT, carried the C-terminal myc tag. (A, top) At 30 h posttransfection, cell lysates were prepared and subjected to luciferase assay. Error bars show the standard deviations (SD) of results from three independent experiments. (A, bottom) Western blot analysis of the cell extracts using anti-myc antibody showed the expression of nsp1, nsp1-CD, and nsp1-mt. Similar levels of actin in each lane, detected by anti-actin antibody, confirmed the loading of similar amounts of cell extracts. (B) Extracted RNAs were subjected to Northern blot analysis using probes that bind to the rLuc gene and endogenous GAPDH RNA.

that both nsp1 and nsp1-CD inhibited rLuc reporter gene expression (Fig. 5A, left). RNA was extracted from the remaining samples after adding the same amount of EMCV IRES-driven EMCV-fLuc RNA, encoding the fLuc gene as a spike RNA, and then it was subjected to a second *in vitro* translation reaction in RRL in the absence of any purified proteins to examine the translational competence of GLA RNA that was extracted from the first *in vitro* translation reaction. We performed this analysis to examine whether nsp1-CD, like nsp1, induced RNA cleavage in GLA RNA in the first *in vitro* translation reaction. Only the GLA RNA that had been incubated with nsp1 in the first *in vitro* translation reaction showed reduced rLuc activity (Fig. 5A, right), demonstrating that nsp1, but not nsp1-CD, induced RNA cleavage in GLA RNA,

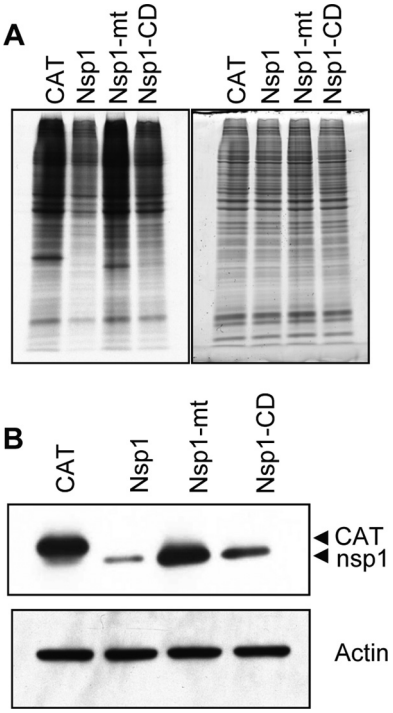

FIG 2 nsp1-CD inhibits host protein synthesis. 293 cells were transfected with RNAs encoding CAT (CAT), nsp1 (nsp1), nsp1-mt (nsp1-mt), or nsp1-CD (nsp1-CD); all of the proteins carried a C-terminal myc epitope tag. The cells were incubated in the presence of actinomycin D from 1 h posttransfection and then labeled with Tran^{35}S-label (MP Biomedicals) from 8.5 to 9.5 h. The cell extracts were subjected to 12% SDS-PAGE gel electrophoresis. (A) The left and right panels show the autoradiographic and the colloidal Coomassie blue-stained image of the gel, respectively. (B, top) Parts of the cell extracts were subjected to Western blot analysis using anti-myc antibody to detect the expression levels of CAT, nsp1, nsp1-mt and nsp1-CD. (B, bottom) The loading of similar amounts of proteins in each lane was confirmed by detecting similar amounts of actin in each lane.

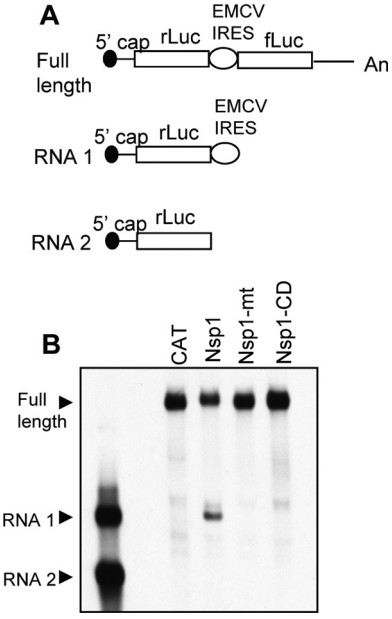

FIG 3 nsp1-CD lacks endonucleolytic RNA cleavage activity. (A) Schematic diagram of the structures of full-length dicistronic Ren-EMCV-FF RNA transcripts (full length), RNA 1, containing the 5′ rLuc gene and intercistronic IRES sequence, and RNA 2, containing only the 5′ rLuc gene. (B) 293 cells were cotransfected with the plasmid encoding Ren-EMCV-FF RNA along with one of the following plasmids: pCAGGS-CAT (CAT), pCAGGS-nsp1 (nsp1), pCAGGS-nsp1-mt (nsp1-mt), or pCAGGS-nsp1-CD (nsp1-CD). At 16 h posttransfection, total RNA was extracted, treated with DNase I, and subjected to Northern blot analysis using digoxigenin-labeled antisense rLuc riboprobe. Full length represents full-length expressed Ren-EMCV-FF RNA, while RNA 1 and RNA 2 represent *in vitro*-synthesized RNA 1 and RNA 2 as shown in panel A. An RNA fragment generated by the nsp1-induced endonucleolytic RNA cleavage was detected in the sample obtained from nsp1-expressing cells.

rendering it translationally inactive. Consistent with these data, nsp1, but not nsp1-CD, induced RNA cleavage in Ren-EMCV-FF RNA in RRL (Fig. 5B) (9, 12). Collectively, these data demonstrated that nsp1-CD bound to the 40S subunit and inhibited mRNA translation but was defective in inducing an endonucleolytic RNA cleavage in the mRNA template.

nsp1-CD inhibits translation initiation complex formation on cap-dependent and IRES-driven template mRNAs. To clarify the translation step inhibited by nsp1-CD, we examined whether nsp1-CD inhibited the translation initiation step by testing the effect of nsp1-CD on the formation of 48S and 80S initiation complexes on cap-dependent and IRES-driven template mRNAs. For testing the effect on cap-dependent mRNAs, we used capped and polyadenylated SCoV mRNA 9, carrying the authentic 5′ UTR of SCoV mRNA 9, and the non-SCoV RNA transcripts, GLA RNA and leaderless rLuc RNA. For IRES-driven mRNA template, we used EMCV IRES-driven EMCV-fLuc RNA. The leaderless rLuc RNA lacks a 5′ UTR and carries only a single G residue at the 5′ end followed by the rLuc gene. Translation initiation on the leaderless rLuc RNA involves the direct loading of the 43S preinitiation complex, composed of the 40S subunit bound to the eIF2–GTP–Met-tRNAiMet ternary complex, eIF1, eIF1A, and eIF3, onto the initiation codon of the rLuc gene. Likewise, initiation on EMCV-fLuc RNA, carrying the 5′ EMCV IRES and the 3′ fLuc gene, also involves the direct recruitment of the 43S complex onto the EMCV IRES. In contrast, translation initiation on GLA RNA carrying a 53-nt-long 5′ UTR and SCoV mRNA 9 carrying the 5′ UTR, including a ~72-nt-long leader sequence, the N gene, and

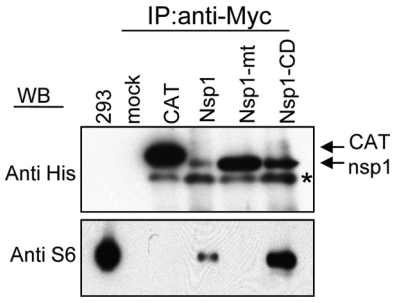

FIG 4 nsp1-CD binds to 40S subunit. Cells were mock transfected (mock) or independently transfected with transcripts encoding CAT, nsp1, nsp1-mt, or nsp1-CD; all proteins carried a C-terminal myc-His epitope tag. At 8 h posttransfection, total cell lysates were prepared, immunoprecipitated with anti-myc antibody followed by stringent washing with high salt buffer, and subjected to Western blotting using an antibody against S6 protein, which is a component of the 40S subunits (termed WB: anti-S6), and anti-His antibody (WB: anti-His). Lysate of 293 cells (293) served as a control. The band that showed migration slightly faster than that of nsp1 was the IgG light chain (asterisk).

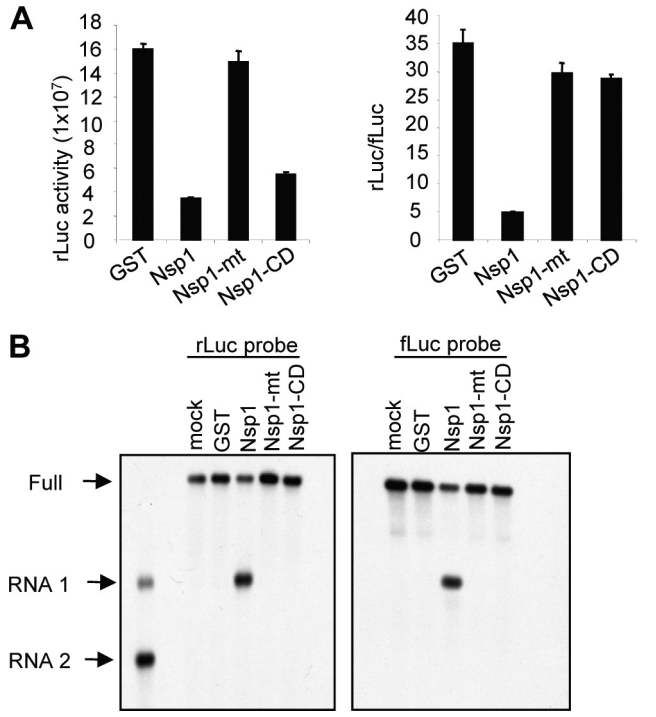

FIG 5 nsp1-CD lacks the endonucleolytic RNA cleavage function. (A) GLA RNA was incubated in RRL in the presence of GST, nsp1, nsp1-mt, or nsp1-CD at 30°C for 20 min. (Left) After incubation, a small aliquot was removed and used to determine rLuc activities. (Right) We spiked the remaining sample with the same amount of EMCV-fLuc RNA, extracted RNAs from the sample, incubated the extracted RNAs in a fresh RRL at 30°C for 30 min, and performed reporter assays. The *y* axis in the right panel represents relative luciferase activity (rLuc/fLuc). Error bars show SD of results from three independent experiments. (B) Ren-EMCV-FF RNA was incubated with GST, nsp1, nsp1-mt, or nsp1-CD or in the absence of protein (mock) in RRL at 30°C for 10 min. After incubation, RNAs were extracted and subjected to Northern blot analysis with probes that bind to the rLuc gene (left) and fLuc gene (right). RNA 1 and RNA 2 represent RNA size markers as described in the legend to Fig. 3.

the 3′-UTR requires scanning by the 43S complex to the AUG initiation codon. Because nsp1 does not induce endonucleolytic RNA cleavage in SCoV mRNAs (12), both nsp1-CD and nsp1 were used for the experiments with SCoV mRNA 9. For the analysis of 48S and 80S complex formation, GMP-PNP and CHX were added, respectively, to the RRL that had been preincubated with GST, nsp1, nsp1-mt, or nsp1-CD. GMP-PNP blocks GTP hydrolysis by eIF2 in eIF2–GTP–Met-tRNAiMet ternary complexes and inhibits the release of eIF2 and subsequent joining of the 60S ribosomal subunit, resulting in arresting translation at 48S complex formation (28), while CHX blocks elongation and arrests translation at the 80S complex stage (23). The samples were incubated with radiolabeled template RNA and subjected to SGC analysis. In addition to SGC analysis, toeprint analysis was also used, in which each template that had been preannealed with the 5′-end-labeled primer was incubated in the RRL samples and then subjected to primer extension without extracting the RNAs. The toeprint, which is a premature primer extension termination signal caused by reverse transcription arrest, for 48S and 80S complexes is produced by the leading edge of the bound 40S subunit ~15 to 17 nt and ~17 to 20 nt downstream of the translation initiation codon, respectively (27); the appearance of the 80S toeprint signal at 20 nt downstream of the translation initiation codon is due to the complete elongation cycle that results in translocation of the first deacylated tRNA from the P site to the E site in the presence of CHX (27, 31).

In both SGC and toeprint analyses, we observed a reduction in the 48S complex formation on leaderless rLuc RNA, GLA RNA, EMCV-fLuc RNA, and SCoV mRNA 9 in the presence of nsp1-CD relative to the respective control samples incubated with GST (Fig. 6). The average percent reduction relative to the GST control for leaderless rLuc RNA, GLA RNA, EMCV-fLuc RNA, and SCoV mRNA 9 was 27 ± 6, 10 ± 2, 38 ± 5 and 11 ± 2, respectively, in SGC analysis and 30 ± 4, 14 ± 1, 40 ± 2 and 8 ± 1, respectively, in toeprint analysis. We detected two 48S toeprint signals, TP-AUG-2 and TP-AUG-3, with EMCV-fLuc RNA (Fig. 6G), and translation generally initiates at the AUG that produces TP-AUG-2 (5, 14). Hence, the reduction in the levels of TP-AUG-2 is presented here.

We also observed a reduction in 80S complex formation on leaderless rLuc RNA, GLA RNA, EMCV-fLuc RNA, and SCoV mRNA 9 in the presence of nsp1-CD relative to the GST control, and the average percent reduction relative to the GST control was 62 ± 5, 53 ± 6, 62 ± 2, and 55 ± 2, respectively, in SGC analysis, and 56 ± 4, 60 ± 3, 66 ± 2, and 43 ± 3, respectively, in toeprint analysis (Fig. 7). Importantly, in both SGC and toeprint analyses, nsp1 and nsp1-CD inhibited 48S and 80S complex formation on SCoV mRNA 9 to a similar extent (Fig. 6D and H and 7D and H), which strongly suggested that nsp1 and nsp1-CD employed the same mechanism to inhibit translation. Overall, the data obtained from SGC and toeprint analyses of a given template were similar. These data revealed that nsp1-CD inhibited both 48S and 80S initiation complex formation with a stronger inhibitory effect on the latter, and the extent of nsp1-CD-mediated inhibition of 48S complex formation was template dependent.

Differential effect of nsp1-CD on binary and 48S and 80S initiation complex formation on RNAs carrying CrPV and HCV IRESes. Translation mediated by both CrPV and HCV IRESes initiates with the binding to 40S subunit to the IRESes to form a binary complex, which occurs in the absence of any translation initiation factors (32). Subsequently, the 60S subunit joins the CrPV IRES-40S binary complex in the absence of any initiation factors to form the 80S complex (38). Binding of eIF3 and the eIF2–GTP–Met-tRNAiMet ternary complex to the HCV IRES-40S binary complex results in the formation of the 48S complex (7, 32, 34), which subsequently proceeds to form the 80S initiation complex using essentially the same mechanisms operating on capped mRNAs. Although translation initiation on capped mRNAs and the IRESes of EMCV, CrPV, and HCV proceeds via different mechanisms, nsp1 inhibits the translation of all of these mRNAs and induces an endonucleolytic RNA cleavage in EMCV IRES and capped non-SCoV mRNAs but not in CrPV IRES, HCV IRES, and SCoV mRNAs (12, 15).

We examined whether nsp1 inhibited translation initiation on RNAs carrying CrPV and HCV IRES by testing the effect of nsp1 on the formation of binary, 48S, and 80S initiation complexes on these RNA templates. To determine the feasibility of examining the effect of nsp1 on binary complex formation, we tested whether nsp1 binds to the purified 40S subunit in the absence of initiation factors. Incubation of nsp1 or nsp1-mt with purified 40S subunits and subsequent sucrose gradient centrifugation analysis showed the cosedimentation

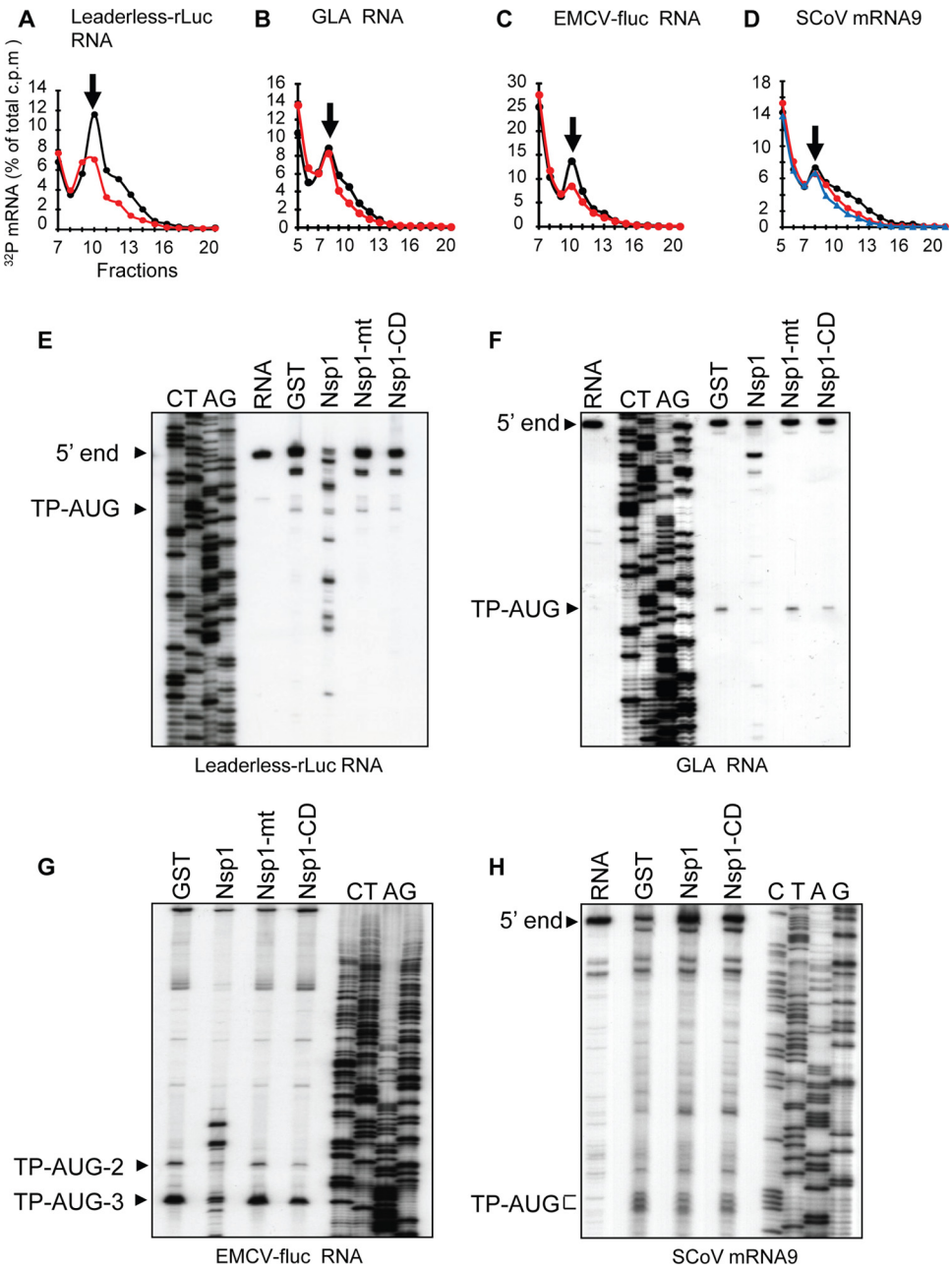

FIG 6 nsp1-CD inhibits 48S complex formation on cap-dependent and IRES-driven mRNAs. (A to D) SGC analysis. RRL was incubated with GST (black), nsp1-CD (red), or nsp1 (blue), and then GMP-PNP was added to the samples. Subsequently, the samples were incubated with radiolabeled leaderless RNA (A), GLA RNA (B), EMCV-fLuc RNA (C), or SCoV mRNA 9 (D) and subjected to SGC analysis. For each graph, fractions toward the bottom of the gradient are represented and fractions from the top of the gradient have been omitted for clarity. Arrows indicate 48S complexes. (E to H) Toeprint analysis. Toeprint analyses were performed using leaderless rLuc RNA (E), GLA RNA (F), EMCV-fLuc RNA (G), and SCoV mRNA 9 (H) in the presence of GST, nsp1, nsp-1-mt, or nsp1-CD. The toeprint of the 48S complex was obtained in the presence of GMP-PNP. For each panel, the same primer that was used for toeprint analysis was also used to sequence the plasmid carrying the corresponding RNA transcripts using the dideoxynucleotide sequencing method. The premature primer extension signals in the samples incubated with nsp1 (except for panel H, where SCoV mRNA 9, which is resistant to the nsp1-induced RNA cleavage, was used) were generated due to the nsp1-induced endonucleolytic cleavage of the template RNAs. RNA, primer extension analysis of the RNA transcripts using the same primer used in each panel; 5′ end, the primer extension product that was extended to the 5′ end of a given RNA; TP-AUG, a correctly positioned toeprint; TP-AUG-2, a correctly positioned toeprint on EMCV IRES; TP-AUG-3, a toeprint on EMCV IRES at AUG that is not used for translation. Each panel shows representative data from at least three independent experiments.

of nsp1, but not nsp1-mt, with 40S subunits, suggesting the initiation factor-independent binding of nsp1 to 40S subunits (Fig. 8).

To identify the step(s) targeted by nsp1 to suppress CrPV IRES-mediated translation, purified 40S subunit, preincubated with GST, nsp1, or nsp1-CD, was mixed with CrPV-fLuc RNA carrying the 5′ CrPV IRES and 3′ fLuc gene and then subjected to SGC and toeprint analyses. SGC analysis showed a reduction in the formation of CrPV-IRES-40S binary complex formation in

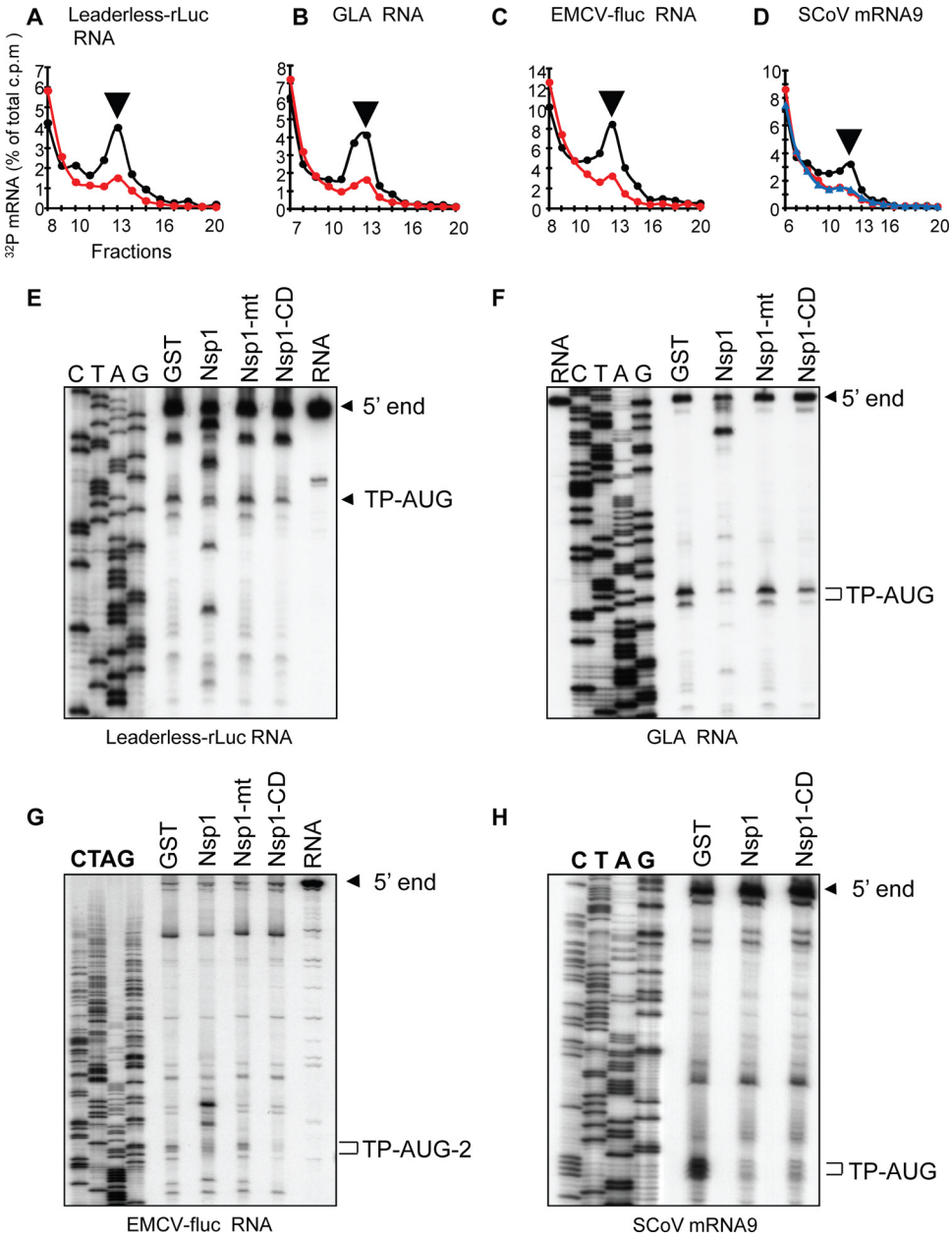

FIG 7 nsp1-CD inhibits 80S initiation complex formation on cap-dependent and IRES-driven mRNAs. Experiments were performed as described in the legend to Fig. 6, except that CHX was added instead of GMP-PNP. Panels A to D and E to H represent SGC analyses and toeprint analyses, respectively. Black, red, and blue lines in A to D represent the samples incubated with GST, nsp1-CD, and nsp1, respectively. Arrowheads in A to D indicate the 80S complexes. TP-AUG, a correctly positioned toeprint; TP-AUG-2, a correctly positioned toeprint on EMCV IRES. Each panel shows representative data from at least three independent experiments.

the presence of nsp1 and nsp1-CD, and the average percent reduction was 67 ± 3 and 65 ± 5, respectively, relative to the control sample incubated with GST (Fig. 9A). Past studies have reported the detection of two toeprints produced by CrPV IRES-40S subunit binary complex (13, 27): a minor toeprint, which we refer to as CrPV toeprint 1, is formed by the interaction of pseudoknot III of the IRES with the 40S subunit, while major CrPV toeprint 2 is produced by the leading edge of the 40S ribosome at nt +15 to +16 downstream of the first nucleotide (+1) of the CCU triplet in the P site. The average percent reduction in the intensity of CrPV toeprint 1 in the presence of nsp1 and nsp1-CD was 18 ± 2 and 13 ± 3, respectively, relative to the control GST sample (Fig. 9B), suggesting only a moderate inhibition of the initial interaction of pseudoknot III with the 40S subunit by nsp1 or nsp1-CD. In contrast, the average percent reduction in the major CrPV toeprint 2 intensities observed in samples incubated with nsp1 and nsp1-CD was 66 ± 3 and 62 ± 4, respectively, relative to the control sample incubated with GST. Collectively, both SGC and toeprint analyses clearly demonstrated that the binding of nsp1 or nsp1-CD to 40S subunits efficiently inhibited the formation of a stable CrPV-IRES-40S binary complex.

We next examined 80S complex formation on CrPV-fLuc

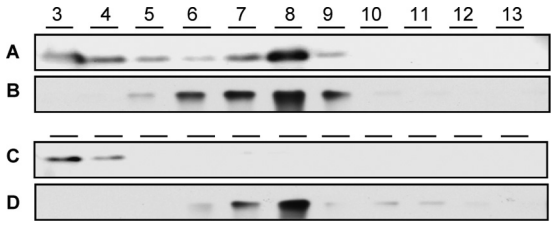

FIG 8 Cosedimentation of nsp1 with 40S subunits. nsp1 (A and B) or nsp1-mt (C and D) was incubated with purified 40S subunits. The samples were subjected to 10 to 40% sucrose density gradient centrifugation. Twenty fractions were collected from the top of the gradient and numbered in ascending order from the top of the gradient to the bottom. (A and C) The presence of nsp1 or nsp1-mt in fractions 3 to 13 was monitored by Western blot analysis with anti-nsp1 antibody. (B and D) The presence of 40S subunits in each fraction was examined by Northern blot analysis using a digoxigenin-labeled oligonucleotide probe that binds to 18S rRNA. The numbers at the top of the panel represent fraction numbers.

RNA in the presence of nsp1 and nsp1-CD using a mixture of purified 40S and 60S subunits. SGC analysis showed an average percent reduction of 63 ± 5 and 60 ± 3 in CrPV-IRES-80S complex formation in the presence of nsp1 and nsp1-CD, respectively (Fig. 9C). Toeprint analysis also showed a reduction in the signal intensities of the 80S toeprint, and the average percent reduction in the presence of nsp1 and nsp1-CD was 56 ± 4 and 53 ± 2, respectively, relative to the GST control (Fig. 9D). These data demonstrated that nsp1 and nsp1-CD inhibited the formation of binary complex and 80S initiation complex on CrPV IRES to a similar extent, implying that nsp1 suppressed CrPV IRES-mediated translation primarily by blocking the formation of stable binary complex on CrPV IRES.

In marked contrast to the strong inhibitory effect of nsp1 on binary complex formation on CrPV-fLuc RNA, both nsp1 and nsp1-CD had a negligible effect on the binary complex formation on HCV-rLuc RNA carrying the 5′ HCV IRES and 3′ rLuc gene (Fig. 9E and F). Remarkably, nsp1 and nsp1-CD efficiently inhibited 48S complex formation on HCV-rLuc RNA in RRL; SGC analysis showed an average percent reduction of 35 ± 5 and 39 ± 4 in 48S complex formation in the presence of nsp1 and nsp1-CD, respectively, relative to the GST control (Fig. 9G), and toeprint analysis showed an average percent reduction of 32 ± 3 and 33 ± 2 with nsp1 and nsp1-CD, respectively (Fig. 9H). The average percent reduction in 80S complex formation with nsp1 and nsp1-CD was 33 ± 3 and 38 ± 2, respectively, relative to the GST control, in SGC analysis (Fig. 9I), and toeprint analysis showed an average percent reduction of 36 ± 1 and 34 ± 3 in the 80S toeprint intensity with nsp1 and nsp1-CD, respectively, relative to the GST control (Fig. 9J). Collectively, the experiments using HCV-rluc RNA revealed that although nsp1 had a negligible impact on the binary complex formation between the HCV IRES and 40S subunits, it efficiently inhibited 48S complex formation on HCV IRES, thereby affecting the assembly of the 80S initiation complex on HCV IRES.

DISCUSSION

The identification of nsp1-CD, which retained the 40S subunit binding and translation inhibitory activity but lacked the mRNA cleavage function of nsp1, allowed us to rule out the effects of mRNA cleavage on translation and dissect the mechanism of nsp1-mediated translation inhibition of mRNAs that are susceptible to nsp1-induced RNA cleavage. Both nsp1 and nsp1-CD exhibited identical inhibitory effects on the translation of mRNAs that are resistant to nsp1-induced RNA cleavage (Fig. 6, 7, and 9), establishing the validity of using nsp1-CD to clarify the mechanism of nsp1-mediated translation inhibition.

Although nsp1-CD did not induce the endonucleolytic cleavage of mRNAs, nsp1-CD expression resulted in the reduction of coexpressed rLuc RNA levels (Fig. 1B). We speculate that nsp1-CD-mediated inhibition of translation initiation could result in the routing of abortive translation initiation complexes at the 48S complex stage to the mRNA triage pathway via stress granules and P bodies, resulting in reduced rLuc RNA levels (2, 4, 10, 21, 25). nsp1 inhibited host protein synthesis more efficiently than nsp1-CD (Fig. 2A), underscoring the contribution of nsp1-induced endonucleolytic mRNA cleavage to host translation inhibition.

nsp1-CD had a strong inhibitory effect on 48S complex formation on scanning-independent leaderless rLuc and EMCV-fLuc RNAs but only a modest inhibition of 48S complex formation on the scanning-dependent GLA RNA and SCoV mRNA 9 (Fig. 6). Differences in the mechanism of translation initiation on these RNA templates could account for the differential inhibitory effect of nsp1-CD. It is conceivable that the binding of nsp1-CD to the 40S subunit induces a conformational change in the 40S subunit such that it inhibits the direct loading of nsp1-bound 43S complex onto leaderless rLuc and EMCV-fLuc RNAs while the scanning competence of the conformationally altered 43S complex is only marginally affected, resulting in a modest inhibitory effect on GLA RNA and SCoV mRNA 9.

Regardless of the differential, template-dependent inhibitory effect of nsp1-CD on 48S complex formation, both nsp1 and nsp1-CD showed a strong inhibitory effect on the 80S complex formation on leaderless rLuc RNA, EMCV-fLuc RNA, GLA RNA, and SCoV mRNA 9 (Fig. 7). These data clearly suggested that nsp1-CD and nsp1 could inhibit at least two separate stages of translation initiation, 48S initiation complex formation and the steps involved in the formation of the 80S initiation complex from the 48S complex. It is possible that nsp1 and nsp1-CD inhibit the assembly of the 80S complex by binding to the 60S subunit-joining interface of the 40S ribosome and sterically hinder the 60S subunit from joining the 48S complex or by inhibiting the functions of eIF5 and/or eIF5B, which are required for the assembly of 80S complex from the 48S complex (32).

nsp1 efficiently inhibited the formation of a stable CrPV IRES-40S binary complex, but it had only a minor effect on the initial interaction of pseudoknot III of CrPV IRES with the 40S subunit (Fig. 9B). It has been proposed that the binding of the 40S subunit to CrPV IRES pseudoknot III induces conformational changes in the 40S ribosome, which facilitate the placement of the GCU triplet in the ribosomal A site (13). nsp1 could interfere with the proposed conformational changes in the 40S ribosome upon loading onto the IRES, thereby preventing the formation of a stable binary complex. Alternatively, nsp1 and CrPV IRES could compete for the binding site in the 40S subunit, thereby sterically hindering the stable CrPV IRES-40S binary complex formation.

In contrast to CrPV IRES, nsp1 did not inhibit the formation of HCV IRES-40S binary complex (Fig. 9E and F). As the binding sites of HCV IRES and CrPV IRES on the 40S subunit are different (33, 34), it is possible that the nsp1 binding site and the HCV IRES binding site on the 40S subunit do not overlap. Although nsp1 did

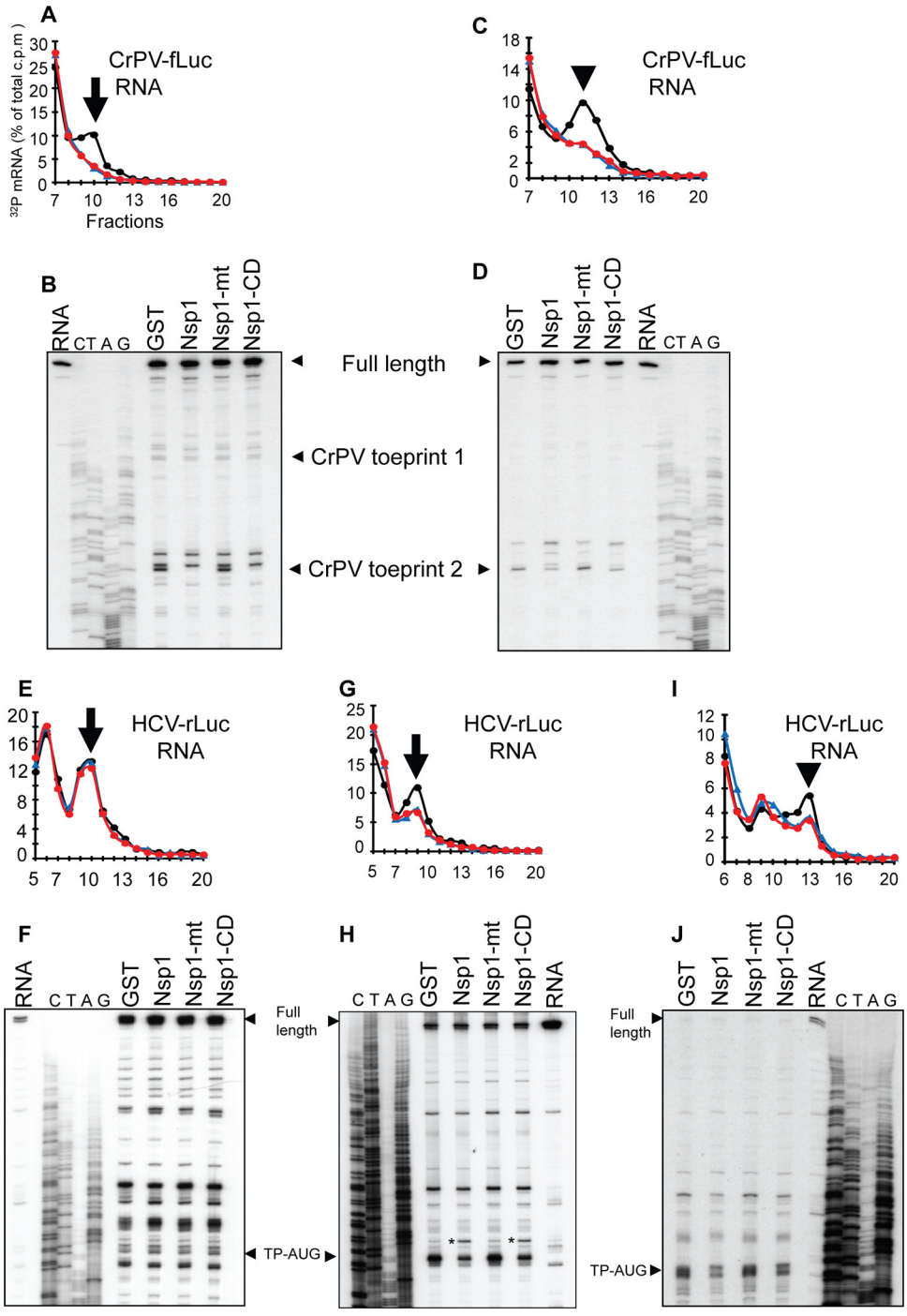

FIG 9 Differential effect of nsp1-CD on binary, 48S, and 80S initiation complex formation on RNAs carrying HCV and CrPV IRESes. Binary complex formation was assayed by incubating GST (black), nsp1-CD (red), nsp1 (blue), or nsp1-mt with purified 40S subunit. Subsequently, the samples were incubated with CrPV-rLuc RNA (A and B) or HCV-rLuc RNA (E and F) and subjected to SGC analysis (A and E) or toeprinting analysis (B and F). SGC (C) and toeprint analyses (D) of 80S complex formation on CrPV-fLuc RNA were performed by incubating purified 40S subunit with GST (black), nsp1-CD (red), or nsp1 (blue) followed by the addition of RNA and purified 60S subunit to the sample. (B and D) The description of CrPV toeprint 1 and toeprint 2 is provided in the text. The SGC and toeprint analyses of 48S (G and H) and 80S complexes (I and J) formed on HCV-rLuc RNA were performed using RRL as described in the legends to Fig. 6 and 7. Arrows indicate binary complex (A and E) or 48S complex on HCV-rLuc RNA (G), while the arrowheads indicate the 80S complexes (C and I). Each panel shows representative data from at least three independent experiments.

not affect HCV IRES-40S binary complex formation, it efficiently inhibited the 48S complex formation on HCV IRES (Fig. 9G and H). The recruitment of eIF2–GTP–Met-tRNAiMet ternary complex and eIF3 to HCV IRES-40S binary complex leads to the formation of 48S complex (8, 32). The presence of nsp1 on the 40S subunit could interfere with the recruitment of the ternary complex and/or eIF3 to the HCV IRES-40S binary complex, thereby inhibiting 48S complex formation. In the toeprint analysis of 48S

complex formed on HCV-rLuc RNA, a relatively strong primer extension signal was also detected at nt +9 downstream of the initiation codon in the samples incubated with nsp1 and nsp1-CD (marked by asterisks in Fig. 9H). A low-intensity signal at the same position was also observed in the absence of RRL (Fig. 9H, RNA) and in samples incubated with GST and nsp1-mt. The stronger intensity of the signal in the presence of nsp1 and nsp1-CD could be due to alterations or stabilization of the putative secondary or tertiary structure in HCV-rLuc RNA induced by the binding of nsp1- and nsp1-CD-altered 40S subunit, leading to efficient reverse transcription arrest in the toeprint analysis.

nsp1-CD and nsp1 exerted a similar inhibitory effect on 48S and 80S initiation complex formation on HCV-rLuc RNA (Fig. 9G to J). Likewise, both nsp1 and nsp1-CD inhibited the binary complex and 80S complex formation on CrPV-fLuc RNA to a similar level (Fig. 9A to D). These data suggest that nsp1 inhibited CrPV-IRES- and HCV-IRES-driven mRNA translation primarily by targeting the steps involved in the formation of binary complex and 48S initiation complex, respectively.

Because the interaction of nsp1-bound 40S ribosome with the mRNA template is required to induce the endonucleolytic RNA cleavage (12), the inability of nsp1-altered 40S ribosome to load onto the mRNA template could be one of the factors governing the resistance of mRNA to nsp1-induced RNA cleavage. Consistent with this model, CrPV IRES-driven mRNA template could be resistant to the nsp1-induced RNA cleavage, as it does not form a stable complex with nsp1-bound 40S subunit (Fig. 9A and B). In contrast, analysis of binary complex and 48S initiation complex formation on HCV IRES-driven mRNA (Fig. 9E to H) and SCoV mRNA 9 (Fig. 6D and H), which are resistant to nsp1-induced RNA cleavage, implied that nsp1-bound 40S subunit can load onto these RNA templates, ruling out the inability of nsp1-bound 40S subunit to load onto these mRNA templates as the mechanism of resistance for these mRNAs. Further studies are required to delineate the mechanism of escape of HCV IRES-driven mRNAs and SCoV mRNAs from nsp1-induced RNA cleavage, although a recent study claimed that the binding of nsp1 to the 5′ UTR of SCoV mRNAs protects the viral mRNAs from nsp1-induced RNA cleavage (35). Collectively, these data pointed to the existence of multiple mechanisms that facilitate the escape of mRNA templates from nsp1-induced RNA cleavage.

ACKNOWLEDGMENTS

We thank Matthias Gromeier for HCV16Luc plasmid and Nicholas Locker for suggestions on SGC analyses.

This work was support by Public Health Service grants AI72493 and AI99107 from the NIH.

REFERENCES

1. **Almeida MS, Johnson MA, Herrmann T, Geralt M, Wuthrich K.** 2007. Novel beta-barrel fold in the nuclear magnetic resonance structure of the replicase nonstructural protein 1 from the severe acute respiratory syndrome coronavirus. J. Virol. **81**:3151–3161.
2. **Anderson P, Kedersha N.** 2008. Stress granules: the Tao of RNA triage. Trends Biochem. Sci. **33**:141–150.
3. **Bordeleau ME, et al.** 2006. Functional characterization of IRESes by an inhibitor of the RNA helicase eIF4A. Nat. Chem. Biol. **2**:213–220.
4. **Dang Y, et al.** 2006. Eukaryotic initiation factor 2α-independent pathway of stress granule induction by the natural product pateamine A. J. Biol. Chem. **281**:32870–32878.
5. **Dmitriev SE, Pisarev AV, Rubtsova MP, Dunaevsky YE, Shatsky IN.** 2003. Conversion of 48S translation preinitiation complexes into 80S initiation complexes as revealed by toeprinting. FEBS Lett. **533**:99–104.
6. **Drosten C, et al.** 2003. Identification of a novel coronavirus in patients with severe acute respiratory syndrome. N. Engl. J. Med. **348**:1967–1976.
7. **Fraser CS, Doudna JA.** 2007. Structural and mechanistic insights into hepatitis C viral translation initiation. Nat. Rev. Microbiol. **5**:29–38.
8. **Fraser CS, Hershey JW, Doudna JA.** 2009. The pathway of hepatitis C virus mRNA recruitment to the human ribosome. Nat. Struct. Mol. Biol. **16**:397–404.
9. **Gaglia MM, Covarrubias S, Wong W, Glaunsinger BA.** 2012. A common strategy for host RNA degradation by divergent viruses. J. Virol. **86**:9527–9530.
10. **Garneau NL, Wilusz J, Wilusz CJ.** 2007. The highways and byways of mRNA decay. Nat. Rev. Mol. Cell Biol. **8**:113–126.
11. **Huang C, et al.** 2011. Alphacoronavirus transmissible gastroenteritis virus nsp1 protein suppresses protein translation in mammalian cells and in cell-free HeLa cell extracts but not in rabbit reticulocyte lysate. J. Virol. **85**:638–643.
12. **Huang C, et al.** 2011. SARS coronavirus nsp1 protein induces template-dependent endonucleolytic cleavage of mRNAs: viral mRNAs are resistant to nsp1-induced RNA cleavage. PLoS Pathog. 7:e1002433. doi:10.1371/journal.ppat.1002433.
13. **Jan E, Sarnow P.** 2002. Factorless ribosome assembly on the internal ribosome entry site of cricket paralysis virus. J. Mol. Biol. **324**:889–902.
14. **Kaminski A, Howell MT, Jackson RJ.** 1990. Initiation of encephalomyocarditis virus RNA translation: the authentic initiation site is not selected by a scanning mechanism. EMBO J. **9**:3753–3759.
15. **Kamitani W, Huang C, Narayanan K, Lokugamage KG, Makino S.** 2009. A two-pronged strategy to suppress host protein synthesis by SARS coronavirus Nsp1 protein. Nat. Struct. Mol. Biol. **16**:1134–1140.
16. **Kamitani W, et al.** 2006. Severe acute respiratory syndrome coronavirus nsp1 protein suppresses host gene expression by promoting host mRNA degradation. Proc. Natl. Acad. Sci. U. S. A. **103**:12885–12890.
17. **Kozak M.** 1998. Primer extension analysis of eukaryotic ribosome-mRNA complexes. Nucleic Acids Res. **26**:4853–4859.
18. **Ksiazek TG, et al.** 2003. A novel coronavirus associated with severe acute respiratory syndrome. N. Engl. J. Med. **348**:1953–1966.
19. **Kuiken T, et al.** 2003. Newly discovered coronavirus as the primary cause of severe acute respiratory syndrome. Lancet **362**:263–270.
20. **Marra MA, et al.** 2003. The genome sequence of the SARS-associated coronavirus. Science **300**:1399–1404.
21. **Mazroui R, et al.** 2006. Inhibition of ribosome recruitment induces stress granule formation independently of eukaryotic initiation factor 2α phosphorylation. Mol. Biol. Cell **17**:4212–4219.
22. **Narayanan K, et al.** 2008. Severe acute respiratory syndrome coronavirus nsp1 suppresses host gene expression, including that of type I interferon, in infected cells. J. Virol. **82**:4471–4479.
23. **Novac O, Guenier AS, Pelletier J.** 2004. Inhibitors of protein synthesis identified by a high throughput multiplexed translation screen. Nucleic Acids Res. **32**:902–915.
24. **Ostareck DH, Ostareck-Lederer A, Shatsky IN, Hentze MW.** 2001. Lipoxygenase mRNA silencing in erythroid differentiation: the 3′UTR regulatory complex controls 60S ribosomal subunit joining. Cell **104**:281–290.
25. **Parker R, Sheth U.** 2007. P bodies and the control of mRNA translation and degradation. Mol. Cell **25**:635–646.
26. **Peiris JS, et al.** 2003. Coronavirus as a possible cause of severe acute respiratory syndrome. Lancet **361**:1319–1325.
27. **Pestova TV, Hellen CU.** 2003. Translation elongation after assembly of ribosomes on the Cricket paralysis virus internal ribosomal entry site without initiation factors or initiator tRNA. Genes Dev. **17**:181–186.
28. **Pestova TV, et al.** 2001. Molecular mechanisms of translation initiation in eukaryotes. Proc. Natl. Acad. Sci. U. S. A. **98**:7029–7036.
29. **Pisarev AV, Unbehaun A, Hellen CU, Pestova TV.** 2007. Assembly and analysis of eukaryotic translation initiation complexes. Methods Enzymol. **430**:147–177.
30. **Rota PA, et al.** 2003. Characterization of a novel coronavirus associated with severe acute respiratory syndrome. Science **300**:1394–1399.
31. **Schneider-Poetsch T, et al.** 2010. Inhibition of eukaryotic translation elongation by cycloheximide and lactimidomycin. Nat. Chem. Biol. **6**:209–217.
32. **Sonenberg N, Hinnebusch AG.** 2009. Regulation of translation initiation in eukaryotes: mechanisms and biological targets. Cell **136**:731–745.
33. **Spahn CM, et al.** 2004. Cryo-EM visualization of a viral internal ribosome entry site bound to human ribosomes: the IRES functions as an RNA-based translation factor. Cell **118**:465–475.

34. **Spahn CM, et al.** 2001. Hepatitis C virus IRES RNA-induced changes in the conformation of the 40s ribosomal subunit. Science **291**:1959–1962.
35. **Tanaka T, Kamitani W, Dediego ML, Enjuanes L, Matsuura Y.** 2012. Severe acute respiratory syndrome coronavirus nsp1 facilitates efficient propagation in cells through a specific translational shutoff of host mRNA. J. Virol. **86**:11128–11137.
36. **Tohya Y, et al.** 2009. Suppression of host gene expression by nsp1 proteins of group 2 bat coronaviruses. J. Virol. **83**:5282–5288.
37. **Wathelet MG, Orr M, Frieman MB, Baric RS.** 2007. Severe acute respiratory syndrome coronavirus evades antiviral signaling: role of nsp1 and rational design of an attenuated strain. J. Virol. **81**:11620–11633.
38. **Wilson JE, Pestova TV, Hellen CU, Sarnow P.** 2000. Initiation of protein synthesis from the A site of the ribosome. Cell **102**:511–520.
39. **Zust R, et al.** 2007. Coronavirus non-structural protein 1 is a major pathogenicity factor: implications for the rational design of coronavirus vaccines. PLoS Pathog. **3**:e109. doi:10.1371/journal.ppat.0030109.